

Ion counting in supercapacitor electrodes using NMR spectroscopy

John M. Griffin, Alexander C. Forse, Hao Wang, Nicole M. Trease, Pierre-Louis Taberna, Patrice Simon, Clare P. Grey

▶ **To cite this version:**

John M. Griffin, Alexander C. Forse, Hao Wang, Nicole M. Trease, Pierre-Louis Taberna, et al.. Ion counting in supercapacitor electrodes using NMR spectroscopy. Faraday Discussions, 2014, 176, pp.49-68. 10.1039/C4FD00138A . hal-02073602

HAL Id: hal-02073602
https://hal.science/hal-02073602

Submitted on 20 Mar 2019

HAL is a multi-disciplinary open access archive for the deposit and dissemination of scientific research documents, whether they are published or not. The documents may come from teaching and research institutions in France or abroad, or from public or private research centers.

L'archive ouverte pluridisciplinaire **HAL**, est destinée au dépôt et à la diffusion de documents scientifiques de niveau recherche, publiés ou non, émanant des établissements d'enseignement et de recherche français ou étrangers, des laboratoires publics ou privés.



Open Archive Toulouse Archive Ouverte (OATAO)

OATAO is an open access repository that collects the work of Toulouse researchers and makes it freely available over the web where possible

This is an author's version published in: **http://oatao.univ-toulouse.fr/23049**

Official URL: https://doi.org/10.1039/C4FD00138A

To cite this version:

Griffin, John M. and Forse, Alexander C. and Wang, Hao and Trease, Nicole M. and Taberna, Pierre-Louis and Simon, Patrice and Grey, Clare P. *Ion counting in supercapacitor electrodes using NMR spectroscopy.* (2014) Faraday Discussions, 176. 49-68. ISSN 1359-6640

Any correspondence concerning this service should be sent to the repository administrator: tech-oatao@listes-diff.inp-toulouse.fr

Ion counting in supercapacitor electrodes using NMR spectroscopy†

John M. Griffin,*[a] Alexander C. Forse,[a] Hao Wang,[a] Nicole M. Trease,[b] Pierre-Louis Taberna,[c] Patrice Simon[c] and Clare P. Grey[ab]

DOI: 10.1039/c4fd00138a

^{19}F NMR spectroscopy has been used to study the local environments of anions in supercapacitor electrodes and to quantify changes in the populations of adsorbed species during charging. In the absence of an applied potential, anionic species adsorbed within carbon micropores (in-pore) are distinguished from those in large mesopores and spaces between particles (ex-pore) by a characteristic nucleus-independent chemical shift (NICS). Adsorption experiments and two-dimensional exchange experiments confirm that anions are in dynamic equilibrium between the in- and ex-pore environments with an exchange rate in the order of tens of Hz. ^{19}F *in situ* NMR spectra recorded at different charge states reveal changes in the intensity and NICS of the in-pore resonances, which are interpreted in term of changes in the population and local environments of the adsorbed anions that arise due to the charge-storage process. A comparison of the results obtained for a range of electrolytes reveals that several factors influence the charging mechanism. For a tetraethylammonium tetrafluoroborate electrolyte, positive polarisation of the electrode is found to proceed by anion adsorption at a low concentration, whereas increased ion exchange plays a more important role for a high concentration electrolyte. In contrast, negative polarization of the electrode proceeds by cation adsorption for both concentrations. For a tetrabutylammonium tetrafluoroborate electrolyte, anion expulsion is observed in the negative charging regime; this is attributed to the reduced mobility and/or access of the larger cations inside the pores, which forces the expulsion of anions in order to build up ionic charge. Significant anion expulsion is also observed in the negative charging regime for alkali metal bis(trifluoromethane)sulfonimide electrolytes, suggesting that more subtle factors also affect the charging mechanism.

[a]*Department of Chemistry, University of Cambridge, Lensfield Road, Cambridge, CB2 1EW, UK. E-mail: jg670@cam.ac.uk; cpg27@cam.ac.uk*

[b]*Department of Chemistry, Stony Brook University, Stony Brook, New York, 11794-3400, USA*

[c]*Université Paul Sabatier Toulouse III, CIRIMAT, UMR-CNRS 5085, F-31062 Toulouse, France*

† Electronic supplementary information (ESI) available. See DOI: 10.1039/c4fd00138a

Electrochemical capacitors, or 'supercapacitors', are currently receiving widespread interest as a promising energy storage technology for high-power applications.[1–3] These devices store charge through electrostatic attraction between ionic charges within an electrolyte and the electronic charge on the electrode surface. Since this mechanism is non-Faradaic, very high charge and discharge rates can be achieved. In addition, since no structural changes take place within the electrode, supercapacitors can offer essentially unlimited cycle lives. Supercapacitor electrolytes typically comprise organic salts such as tetraethylammonium tetrafluoroborate (NEt_4–BF_4) dissolved in acetonitrile (ACN).[3] Such electrolytes offer high ionic conductivity and higher breakdown voltages than aqueous electrolytes, enabling more energy to be stored. There has also been an increasing focus on the use of room-temperature ionic liquids as supercapacitor electrolytes, as they offer greater thermal stability than organic electrolytes and have an even wider voltage window.[4–6] Supercapacitor electrodes are generally constructed using porous carbon due to its high surface area and conductivity.[7] In particular, porous carbon derived from organic precursors such as coconut shells and wood are widely used due to their low cost and high availability. These materials are predominantly microporous with pore sizes in the range 1–2 nm, although they can also exhibit a range of pore sizes in the mesoporous and macroporous regimes. The importance of the relationship between pore size and ion size was highlighted by Chmiola *et al.*, who reported an anomalous increase in capacitance for microporous titanium carbide-derived carbons with pore sizes that were smaller than the solvated ion size.[8] This challenged the previously-held view that pores smaller than the solvated ion size do not contribute significantly to the capacitance. It has been hypothesized that ion desolvation results in a closer proximity of the charge centres to the electrode surface, resulting in higher capacitance.[9] However, experimental validation of this hypothesis is scarce, and many questions relating to the mechanism of supercapacitance in general remain unanswered. A better understanding of this important phenomenon will lead to the design of devices with improved properties.

To gain insight into the mechanism of supercapacitance, a large number of theoretical studies have been carried out. Huang *et al.* developed theoretical models based upon a so-called electric-double cylinder and electric wire-in-cylinder capacitors in order to correlate capacitance with properties such as pore size, specific surface area and ion size.[10] Kondrat *et al.* have used mean field theory models to propose that image charges arising from the charged micropore surfaces facilitate the packing of ions of the same polarity during charging, accounting for the large increases in capacitance experimentally measured for carbons with micropores smaller than the solvated electrolyte ions.[11,12] A large amount of theoretical insight has also been gained through the application of molecular dynamics simulations.[13–15] In particular, these studies have revealed the importance of the overscreening effects at planar electrode–electrolyte interfaces, which give rise to the layering of ions in an oscillatory pattern, whereby capacitance decays with increasing pore size.[16–19] It has been suggested that the absence of such effects in microporous electrodes allows high capacitances to develop.[20]

A range of experimental methods have also been employed in order to study the structure of the electrode–electrolyte interface in supercapacitors. Neutron diffraction has been used to observe and quantify ion diffusion and concentration variations as a function of the applied potential.[21,22] Changes in electrolyte absorbances measured in *in situ* infrared spectroscopy experiments have been attributed to the net movement of positive and negative ion pairs into carbon micropores upon charging.[23] Changes in the height of electrodes in electrochemical dilatometry experiments have been interpreted in terms of shrinkage and expansion of pores as ions fill and leave the electrode.[24] Recently, a number of studies have demonstrated the utility of *in situ* electrochemical quartz crystal microbalance methodologies to track changes in electrode mass during charging and discharging.[25–28] Deviations from theoretical mass changes based on Faraday's law have been interpreted in terms of distinct charging regimes, which are characterized by the compositional differences in the ionic part of the electric double layer. For aqueous and organic electrolytes, these studies have generally identified two distinct charging regimes for the systems studied; at low potentials charging was found to proceed *via* ion exchange, whereas at high potentials counter-ion adsorption plays a more dominant role. Recently, this approach has been extended to the study of ionic liquids where similar observations were reported for the positive polarisation of the electrode, whereas for negative polarisation the observed mass change was consistent with adsorption of counter-ions only across the voltage range studied.[28]

Despite the progress that has been made in both theoretical and experimental methods for the study of supercapacitance, further work is required to fully understand this complex process. In particular, the development of experimental methods that can selectively observe and quantify anions or cations will add significant insight. In this respect, nuclear magnetic resonance stands out as a highly localised and element-selective probe of chemical environments. A number of early studies by Harris *et al.* demonstrated the potential of NMR for the study of molecules adsorbed on porous carbon, where distinct resonances were observed for adsorbed and non-adsorbed species within activated carbons.[29–31] Subsequent studies on a range of different carbon morphologies have revealed similar trends, whereby resonances corresponding to species adsorbed on the carbon surface are always observed at a lower frequency than their non-adsorbed counterparts, regardless of the species studied.[32–39] This effect has also been investigated in theoretical studies, where it has been shown that the characteristic shift in frequency for adsorbed species arises due to the circulation of delocalised electrons in the carbon surface, which results in a locally reduced magnetic field.[40–43] This so-called nucleus-independent chemical shift (NICS) therefore provides a useful means by which to identify ions confined within carbon micropores and can in principle be used to obtain information about their local chemical environments such as pore diameter and local curvature of the carbon surface. Indeed, we have recently shown how NMR can identify adsorbed ions in model supercapacitor electrodes comprising pieces of microporous carbon film soaked with a NEt_4–BF_4/ACN electrolyte.[38,39] Furthermore, since NMR is in principal a quantitative technique (*i.e.*, the integrated spectral resonance intensity is directly proportional to the number of species in a particular chemical environment), it can be used to monitor changes in adsorbed ion populations during charging. Recent work has shown how magic-angle spinning (MAS) NMR

experiments can identify differences in the number, and local environments, of ions in electrodes taken from supercapacitors that were disassembled at different charge states.[44] To obtain a direct insight into working supercapacitor devices under realistic charging conditions, *in situ* NMR methods have also been developed. These approaches involve the use of a specially-designed supercapacitor cell which is situated inside the NMR spectrometer, enabling the acquisition of NMR spectra under a range of charging conditions. We have recently demonstrated the utility of this approach whereby systematic changes were observed in ^{11}B NMR spectra of a supercapacitor comprising a NEt_4–BF_4/ACN electrolyte and activated carbon electrodes which were held at different applied potentials.[38] Through the use of ^{19}F NMR spectroscopy, this approach was further developed to enable the quantification of relative adsorbed anion populations at different charge states, and the observation of changes in anion environments under dynamic charging conditions.[45]

Having developed and refined the *in situ* NMR methodology for the study of supercapacitors, the focus of the current study is to apply this approach to build up an understanding of different factors that affect the charging mechanism. We first investigate the effects of electrolyte concentration on the adsorption of anions in model electrodes in the absence of an applied potential. We then measure changes in the number and local environment of the adsorbed anions when a potential is applied to a working supercapacitor device. This reveals important information about the charge storage process in each system, and by comparing a range of different electrolytes it is possible to correlate the observed differences with the properties of the electrolyte, such as concentration and relative ion size.

Experimental details

Materials

All carbon electrodes were prepared from YP-50F activated carbon (Kuraray Chemical, Japan). Free-standing carbon films were prepared in the standard way[46] by mixing carbon powder (95 wt%) with polytetrafluoroethylene (5 wt%) (Sigma Aldrich, 60 wt% dispersion in water). The films were rolled to an approximate thickness of 0.25 mm. Prior to sample preparation, carbon film pieces were dried under vacuum at 200 °C overnight and then transferred to an argon glove box with H_2O and O_2 levels less than 0.1 ppm. Inside the glove box, the film pieces were cut to the specified mass with the approximate dimensions 4 × 10 mm. The electrolyte salts used were tetraethylammonium tetrafluoroborate (NEt_4–BF_4, Sigma Aldrich, electrochemical grade >99.0%), tetrabutylammonium tetrafluoroborate (NBu_4–BF_4, Sigma Aldrich, >99.0%), lithium bis(trifluoromethane)sulfonimide (Li-TFSI, 3M HQ-115) and sodium bis(trifluoromethylsulfonyl)imide (Na-TFSI), synthesized by neutralizing bis(trifluoromethylsulfonyl)imide (Iolitec GmbH, >98%) with excess sodium carbonate, followed by drying *in vacuo* and filtration with dry ACN.

Sample preparation

All bag cell samples were prepared inside an argon glove box with H_2O and O_2 levels less than 0.1 ppm. Model electrodes were prepared by sealing a carbon film

piece inside a plastic bag (3M packaging film) with the chosen volume of electrolyte, which was added using a microsyringe. All model supercapacitor cells in this study were also constructed using plastic bag cell designs with 'overlaid' electrode configurations as discussed in detail in ref. 45: carbon film pieces were pressed onto strips of carbon-coated aluminium mesh, and a Celgard 2500 (monolayer polypropylene, 25 μm thickness) separator was placed between them. These components were placed inside a plastic bag (3M packaging film), which was heat sealed on three sides. The cell was then filled with electrolyte before making the final seal to close the bag. For NMR measurements, the supercapacitor bag cells were held between two rigid plastic strips inside the NMR coil in order to provide rigidity and allow better control over the cell orientation.

NMR details

Adsorption studies and *in situ* NMR experiments were performed using a Bruker Avance spectrometer operating at a magnetic field strength of 7.05 T, corresponding to a ^{19}F Larmor frequency of 284.2 MHz. A Bruker HX double resonance static probe was used, with a 6.8 mm inner diameter solenoid coil. The "depth" pulse sequence[47] with a 90° pulse length of 5.5 μs was used in order to reduce the background signal from the PTFE probe-head housing. The total delay between excitation of transverse magnetization and acquisition of the free induction decay was 90 μs. A recycle interval of 30 s was used, which was sufficient for the spectra to be quantitative. ^{19}F exchange MAS NMR experiments were carried out using a Bruker Avance spectrometer operating at a magnetic field strength of 9.4 T, corresponding to a ^{19}F Larmor frequency of 376.6 MHz. A Bruker 2.5 mm probe was used, and all experiments were performed at a MAS rate of 5 kHz with a 90° pulse length of 3.5 μs. For each exchange experiment, either 8 transients (1.5 M electrolyte) or 16 transients (0.5 M electrolyte) were coadded for each of the 160 t_1 increments. A short recycle interval of 2 s was used in order to enable the acquisition of multiple two-dimensional spectra within a reasonable time. For each experiment, 3 μL of electrolyte was added to 4 mg of film inside the MAS rotor. All ^{19}F NMR spectra are referenced relative to neat hexafluorobenzene (C_6F_6) at −164.9 ppm.

In situ NMR methodology

In situ experiments were carried out by placing the pristine cell in the NMR coil in the vertical orientation[39] and charging sequentially to a series of different voltages (0, 0.25, 0.5, 0.75, 1, 1.25, 1.5, 0, −0.25, −0.5, −0.75, −1, −1.25 and −1.5 V). The applied potential was controlled using a Bio-logic cycler in a two-electrode configuration. The cells were held at each voltage until a constant current was obtained, and then the ^{19}F NMR spectra were acquired; in most cases this was 45–60 minutes, while for NBu_4–BF_4 90 minutes was required. For the discharge of the cell (1.5 → 0 V), current relaxations of double duration were used. Spectral fitting was carried out using DMfit software.[48] Deconvolutions were carried out as described previously in ref. 45. Some spectra required several lineshapes to describe the free electrolyte/ex-pore resonance. This is ascribed to local variations in the magnetic field across the bag cell due to the different susceptibilities of the cell components, which results in a range of different local fields and thus shifts for the same chemical species.[45] For this reason, it is not necessarily appropriate

to assume purely Lorentzian lineshapes for the ex-pore feature (as would be expected for an isotropic liquid in a homogeneous magnetic field), and so multiple lineshapes with mixtures of Gaussian and Lorentzian components were used to accurately model this feature. Similarly, the lineshape of the in-pore feature is expected to be influenced by both local field variations, motional effects, and distributions of the chemical environments, and so the Gaussian/Lorentzian ratio for this feature was allowed to vary. In some cases, the fitting routine gave unrealistic values for the Gaussian/Lorentzian ratio for some components (*i.e.*, less than 0 or greater than 1); in these cases, the ratios were fixed to either 0 or 1 and the fit was repeated. For each electrolyte, the spectrum obtained at 0 V was fitted first, as this showed the best resolution of the in-pore resonance. The peak positions and intensities obtained were then used as a starting point to fit the spectrum at the next highest voltage. Fits were repeated two or three times for each series of data in order to estimate errors. Representative deconvolutions and deconvolution parameters are given in the ESI.†

Results

Adsorption of BF_4 anions at zero applied potential

We first investigate factors affecting anion adsorption in porous carbon in the absence of an applied potential. While ^{1}H NMR is an attractive option for the study of organic tetra-alkylammonium cations, the large number of plastic components used in the bag cell assembly results in a broad and intense background ^{1}H signal that precludes the observation of the relatively low intensity

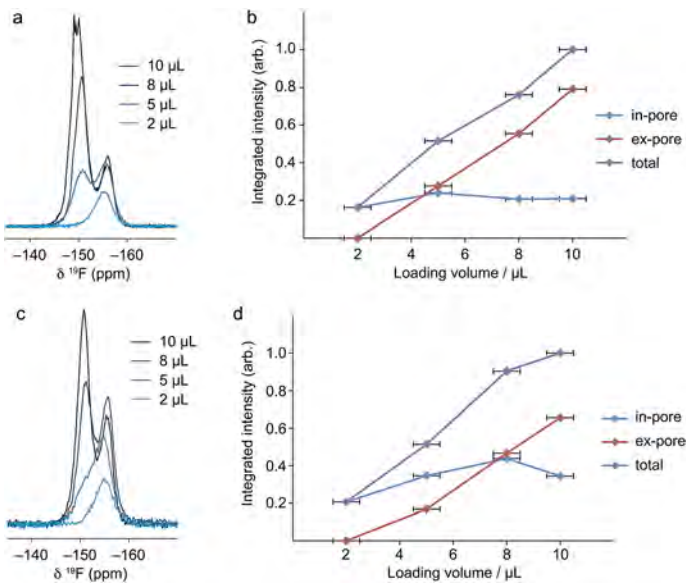


Fig. 1 ^{19}F NMR spectra of 4 mg YP-50F carbon films with different amounts of (a) 1.5 M NEt_4–BF_4/ACN and (c) 0.5 M NEt_4–BF_4/ACN electrolyte in plastic bags. Deconvoluted relative integrated intensities for the two main resonances are shown in (b) and (d).

electrolyte resonances. For this reason, we focus this study on ^{19}F NMR which provides a probe of the fluorine-containing anions.[38,45]

Fig. 1a shows ^{19}F NMR spectra of 4 mg YP-50F carbon films soaked with different amounts of 1.5 M NEt_4–BF_4/ACN electrolyte. Across the series of spectra, two main resonances are observed. Deconvoluted intensities determined for the two resonances at each loading volume are shown in Fig. 1b. For the lowest loading volume of 2 μL, the single resonance observed at −155 ppm corresponds to the BF_4 anions that are adsorbed to the carbon surface inside the micropores (referred to hereafter as 'in-pore'). As more electrolyte is added, the intensity of the in-pore resonance increases but then saturates around a loading volume of 5 μL. Simultaneously, a second resonance is observed at −150 ppm which corresponds to the BF_4 anions that are situated outside of the micropores (hereafter referred to as 'ex-pore'). As more electrolyte is added, the ex-pore resonance continues to grow, while there appears to be a small reduction in the in-pore resonance intensity. Fig. 1c and d show ^{19}F NMR spectra and integrated resonance intensities for films soaked in the same electrolyte at a lower concentration of 0.5 M. The spectra also exhibit in-pore and ex-pore resonances, although the relative build up rates of the two environments as a function of loading volume are slightly different. For this system, saturation of the in-pore resonance intensity occurs at around 8 μL, and there is a noticeable decrease in intensity of this resonance at the next loading volume of 10 μL.

Comparison of the adsorption behaviour for the two concentrations provides insight into the nature of the adsorption process. YP-50F has a specific surface area of 1600 $m^2\ g^{-1}$ and a total pore volume of approximately 0.7 $cm^3\ g^{-1}$, according to data supplied by the manufacturer.[49] According to gas adsorption measurements, 46% of the pore volume is less than 1 nm in size, 46% is between 1–2 nm, and the rest is greater than 2 nm.[50] For NEt_4–BF_4, solvated ion diameters are 1.16 nm (BF_4^-) and 1.30 nm (NEt_4^+),[9] meaning that ions can easily access a large fraction of the pores. For a 4 mg piece of YP-50F film, the total pore volume is estimated to be between 2.7–3.3 μL. For the 1.5 M electrolyte at the highest loading volume of 10 μL, 16% of the anions are found to occupy the in-pore environment, corresponding to 3.1 μmol of anions. Assuming equal adsorption of anions and cations, the total volume occupied by in-pore electrolyte ions in this sample is estimated to be 3.67 μL on the basis of the solvated ion diameters. This value is slightly higher than the estimated total pore volume of the film piece, and may therefore indicate partial desolvation or overlap of anion and cation solvation shells inside the pores. Indeed, a recent electron radial distribution function study has indicated that electrolyte solvent molecules can become partially aligned when confined within sub-nanometre pores in activated carbon.[51] For the 0.5 M electrolyte at a loading volume of 10 μL, 34% of anions (corresponding to 1.7 μmol) occupy the in-pore environment. Again assuming equal adsorption of anions and cations, the total volume taken up by the solvated ions is estimated to be 2.01 μmol. The packing density of the ions inside the pores is therefore reduced for the lower concentration electrolyte, being approximately equal to 0.55 times that of the high concentration electrolyte. However, the packing density is reduced by less than a factor of 2/3, which may be expected based on the ratios of the concentrations, indicating that there is still a preference for anions to occupy the in-pore rather than the ex-pore environment. Overall, these results show that for electrolyte volumes smaller than the total pore volume, all of the electrolyte

occupies the space within the micropores. When the loading volume exceeds the total pore volume, larger voids in the carbon become filled with electrolyte and ions start to be distributed between the in- and ex-pore environments. The observed decreases in the number of in-pore anions at high loading volumes indicate that the equilibrium between the occupation of the in- and ex-pore environments changes slightly as more ex-pore reservoirs become accessible. For the high concentration electrolyte, the ions are densely packed within the micropores at a high loading volume.

To further investigate the nature of the equilibrium between the occupation of the in-pore and ex-pore environments, ^{19}F two-dimensional exchange (2D-EXSY) NMR spectra were recorded. The ^{19}F 2D-EXSY NMR experiments measure the retained magnetization as the BF_4 anions exchange between in-pore and ex-pore environments during a mixing time, t_m. The spectra were recorded under magic-angle spinning (MAS) conditions in order to improve the resolution between the in-pore and ex-pore resonances. Representative spectra for YP-50F film soaked with 1.5 M NEt_4–BF_4/ACN are shown in Fig. 2a and b. Using a short t_m of 0.5 ms (Fig. 2a), only resonances on the autocorrelation diagonal are observed, showing that there is no movement of anions between the in-pore and ex-pore environments on this timescale. Using a much longer t_m of 50 ms (Fig. 2b), significant off-diagonal cross peak intensity is observed correlating to the in-pore and ex-pore resonances, showing that the exchange of anions between these environments takes place. By recording a set of 2D-EXSY NMR spectra with a range of t_m values, it is possible to estimate a rate constant, k, for a two-site exchange process by fitting integrated off cross-peak/diagonal-peak intensities to

$$\frac{a_{\text{cross}}}{a_{\text{diag}}} = \tanh(kt_m) \quad (1)$$

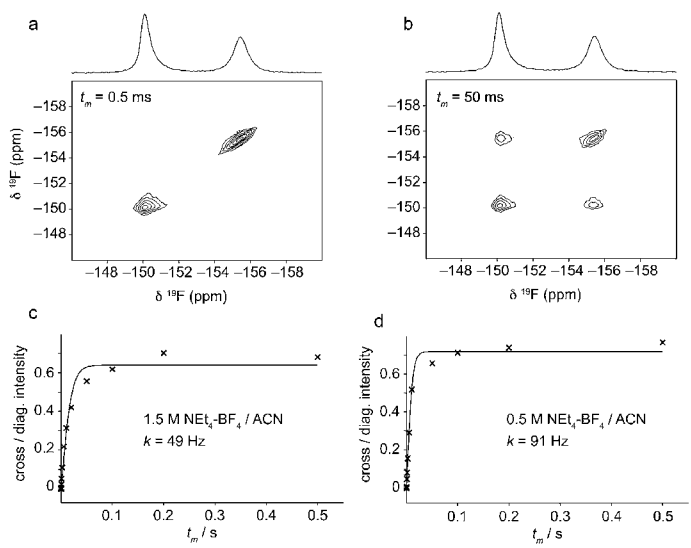


Fig. 2 ^{19}F 2D-EXSY NMR spectra of the YP-50F film soaked with 1.5 M NEt_4–BF_4/ACN electrolyte recorded with mixing times of (a) 5 ms and (b) 50 ms. Fits to the cross-peak/diagonal-peak intensity ratio as a function of t_m are shown for 1.5 M and 0.5 M NEt_4–BF_4/ACN electrolytes in (c) and (d), respectively.

where a_{cross} is the cross-peak intensity and a_{diag} is the diagonal-peak intensity.[52] Fits to the data obtained for the YP-50F film soaked with both 1.5 M and 0.5 M NEt_4–BF_4/ACN are shown in Fig. 2c and d, respectively. For 1.5 M NEt_4–BF_4/ACN, exchange between the in-pore and ex-pore environments is found to take place with a rate constant of 49 Hz, while for the lower concentration a higher rate constant of 91 Hz occurs. We note that the fits do not exactly reproduce the experimental data at long t_m values. This is likely to be due to the differences in longitudinal relaxation times between the in- and ex-pore environments,[38] and the fact that in reality the dynamic processes in these systems are taking place across a range of time- and length-scales. In-pore anions located near the edge of the microporous carbon particles will exchange with the ex-pore environment on a faster timescale than anions located near the centre of the carbon particles, which first need to diffuse to the edge. Since the NMR spectra do not distinguish ions near the edges and centres of the carbon particles, the observed exchange effects will be the superposition of the intraparticle diffusion process and the in-pore–ex-pore exchange process. However, the measured rate constants do provide an indication of the timescale of the in-pore–ex-pore exchange process in each system and show that a faster exchange takes place in the lower concentration electrolyte.

^{19}F *in situ* NMR of supercapacitor electrodes under applied potentials

To gain insight into the changes in the populations and local environments of the in-pore anions during charging, ^{19}F *in situ* NMR experiments were carried out on supercapacitor cells held at fixed voltages between −1.5 and 1.5 V. For each experiment, the cell was first held at 0 V, and the applied cell voltage was then increased in steps of 0.25 V to a maximum value of 1.5 V. The cell was then discharged to 0 V in a single step, before the applied voltage was changed in steps of −0.25 V to a maximum value of −1.5 V. At each voltage, a ^{19}F NMR spectrum was recorded after the cell current had fully relaxed. Gravimetric capacitances for each cell as determined from the integration of the total discharge current for the 1.5 → 0 V step are summarised in Table 1.

Fig. 3a and b show ^{19}F *in situ* NMR spectra recorded for a supercapacitor cell containing 1.5 M NEt_4–BF_4/ACN electrolyte. At 0 V, the in-pore resonance is observed at −155.0 ppm together with an intense feature centred around −148 ppm, which correspond to the ex-pore and free electrolyte anions. As the applied voltage is increased, the in-pore resonance moves to a higher frequency and appears to increase in intensity. The ex-pore/free electrolyte feature does not

Table 1 Gravimetric capacitances determined from the 1.5 → 0 V discharge for each system studied in this work

Electrolyte	Gravimetric capacitance/F g^{-1}
1.5 M NEt_4–BF_4/ACN	101.3
0.5 M NEt_4–BF_4/ACN	97.7
1.5 M NBu_4–BF_4/ACN	97.2
1.5 M Li-TFSI/ACN	95.1
1.5 M Na-TFSI/ACN	92.7

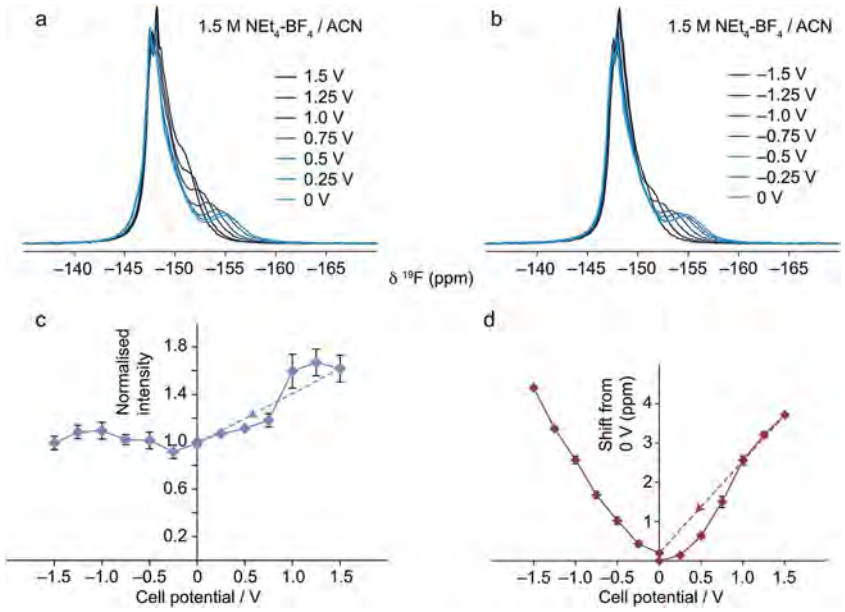


Fig. 3 ^{19}F *in situ* NMR spectra of the supercapacitor electrode containing 1.5 M NEt_4–BF_4/ACN electrolyte charged to potentials between (a) 0 and 1.5 V and (b) 0 and −1.5 V. Deconvoluted in-pore resonance intensities and shift differences are shown in (c) and (d), respectively. Lines are added as guides for the eye. Dotted arrows indicate the 1.5 V → 0 V discharge step.

display significant changes upon charging. After discharging to 0 V, the in-pore resonance returns to close to its original position at −154.8 ppm. As the applied voltage is then increased towards −1.5 V, the in-pore resonance again shifts to a high frequency; however, the changes in intensity are much less pronounced than for the positive charging regime. These observations are consistent with results reported previously for a similar system.[45] It was shown that changes in the intensity of the in-pore resonance correspond to changes in the in-pore anion population as anions are adsorbed or expelled from the electrode during charging. Changes in the frequency of the in-pore resonance arise due to changes in the electronic structure of the carbon as electrons are added to or removed from the electrode during charging. Interestingly, the in-pore resonance shifts in the same direction during charging and discharging. This is consistent with DFT calculations of NICS values for positively- and negatively-charged model carbon fragments.[45] Deconvoluted intensities and shifts for the in-pore resonance, shown in Fig. 3c and d, give a more precise picture of the changes in the in-pore anion population and local environment. In the positive charging regime the intensity of the in-pore resonance increases throughout the voltage range as anions are adsorbed inside the pores, although a 'jump' in intensity is observed at around 1 V. In contrast, the total charge stored in the supercapacitor, as determined from integration of the current relaxation, was found to vary approximately linearly with voltage step (see the ESI†). This was also observed previously,[45] and suggests a transition between two different charge storage processes. At a low voltage, the

relatively small changes seen in the in-pore anion population indicate that charge is being stored at least in part through the expulsion of cations from the pores (which are not observed in the ^{19}F NMR spectra). At a high voltage, the abrupt increase in the in-pore anion resonance shows that charge storage is increasingly being achieved through the adsorption of anions. At 1.5 V, the in-pore anion population is approximately 1.6 times that at 0 V. When the capacitor is discharged to 0 V, the in-pore resonance returns to its original intensity showing that the additional adsorbed anions are released from the pores as the system returns to equilibrium. A small hysteresis in the shift of the in-pore resonance is observed, indicating that the charging process may result in small irreversible changes in the electrode (such as oxidation or reduction of the functional groups, or reactions involving electrolyte species). However, we note that the total charge and discharge currents are almost identical (Fig. S2†), showing that the extent of any irreversible processes must be small. Across the negative voltage range, very little overall change in the intensity of the adsorbed resonance is observed. However, the integration of the charging current (Fig. S2†) and the observed change in shift of the in-pore resonance confirm that a similar amount of charge is stored in this voltage range. This indicates that charge storage must take place through the adsorption of cation into the micropores, while the number of anions inside the pores remains relatively constant.

Fig. 4a and b show the ^{19}F *in situ* NMR spectra recorded for the analogous supercapacitor cell containing 0.5 M NEt_4–BF_4/ACN electrolyte. For this system, the in-pore resonance is again observed to change intensity and shift to a high frequency during charging. However, the deconvoluted resonance intensities shown in Fig. 4c reveal that the relative intensity changes in the positive voltage range are much more pronounced than for the higher concentration electrolyte. Between 0 and 1.5 V, the intensity of the in-pore resonance increases by a factor of approximately 3.2. At the same time, the total change in resonance frequency of 3.6 ppm over this range (Fig. 4d), and the gravimetric capacitance (Table 1), are similar to that observed for the higher concentration electrolyte, showing that the total amount of charge stored is not significantly affected. If it is assumed, on the basis of the NMR adsorption experiments, that the packing density of the ions inside the electrode for the 0.5 M electrolyte at 0 V is 0.55 times that of the 1.5 M electrolyte, then the relative increase factors of 3.2 (0.5 M electrolyte) and 1.6 (1.5 M electrolyte) indicate that approximately twice as many anions are adsorbed in the low concentration electrolyte as compared to the high concentration electrolyte. If at 0 V equal adsorption of anions and cations is assumed, the higher number of cations present at 0 V in the 1.5 M electrolyte means that some proportion must be expelled from the pores in order to build up a similar total ionic charge to the 0.5 M electrolyte. This suggests that for positive polarization of the electrode, anion adsorption plays a more important role in the charge storage process at low concentrations, while ion exchange takes place at higher concentrations. When the supercapacitor is discharged to 0 V, the intensity of the in-pore resonance remains slightly higher than for the pristine state and a small hysteresis in the shift is observed, again indicative of small irreversible changes in the electrode. As the cell is charged to −1.5 V, very little change is observed in the in-pore anion intensity, while the resonance frequency again changes by 3.7 ppm. This suggests that, as is the case for the higher concentration electrolyte, the

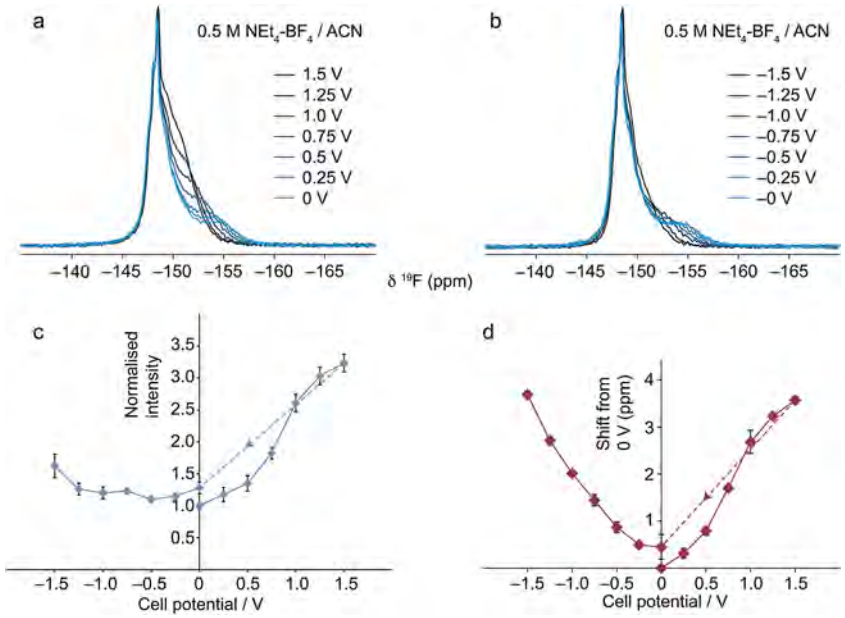


Fig. 4 ^{19}F *in situ* NMR spectra of a supercapacitor electrode containing 0.5 M NEt_4–BF_4/ACN electrolyte charged to potentials between (a) 0 and 1.5 V and (b) 0 and −1.5 V. Deconvoluted in-pore resonance intensities and shift differences are shown in (c) and (d), respectively. Lines are added as guides for the eye. Dotted arrows indicate the 1.5 V → 0 V discharge step.

charging storage mechanism in the negative voltage range largely involves cation adsorption only.

Fig. 5 shows the ^{19}F *in situ* NMR spectra and deconvoluted in-pore resonance intensities and shifts for the supercapacitor cell containing 1.5 M NBu_4–BF_4/ACN electrolyte. In this system, the same BF_4 anions are present but the NBu_4 cations are significantly larger, with an estimated desolvated diameter of 1.1 nm (based on an X-ray crystal structure for tetrabutylammonium hydrogen sulphate[53]), as compared to 0.67 nm for NEt_4^+.[9] Across the positive voltage range, a steady increase in the in-pore anion intensity is observed. The gravimetric capacitance (Table 1) and the total shift change of 3.1 ppm (Fig. 5d) are very similar to the NEt_4–BF_4 electrolytes. However, the factor of 1.3 increase in the in-pore anion population is slightly less than was observed for the 1.5 M NEt_4BF_4 electrolyte, suggesting that the degree of cation expulsion is slightly higher in this system. After discharging to 0 V, there is a noticeable reduction in the intensity of the in-pore anion resonance as compared to the pristine state, and a small hysteresis in the shift. However, the integrated charge and discharge currents over the positive charging range are again almost identical (Fig. S2†), showing that the charging process is largely reversible. It is possible that the bulky cations have difficulty re-entering the pores after charging, and so slightly more anions are expelled from the pores to maintain local charge neutrality. As the capacitor is charged to −1.5 V, a considerable reduction in the in-pore resonance intensity is observed, showing that for this electrolyte the anions are expelled from the electrode under

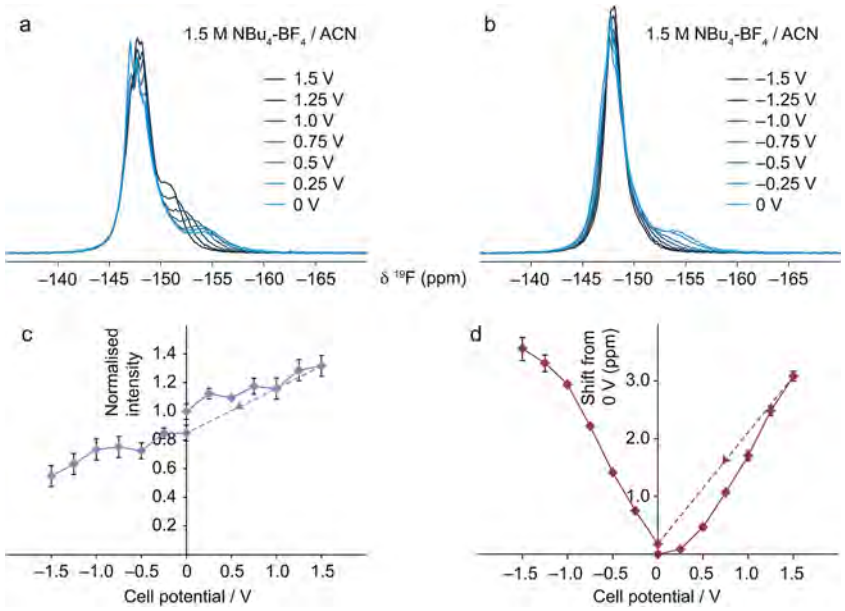


Fig. 5 ^{19}F *in situ* NMR spectra of a supercapacitor electrode containing 1.5 M NBu_4–BF_4/ACN electrolyte charged to potentials between (a) 0 and 1.5 V and (b) 0 and −1.5 V. Deconvoluted in-pore resonance intensities and shift differences are shown in (c) and (d), respectively. Lines are added as guides for the eye. Dotted arrows indicate the 1.5 V → 0 V discharge step.

negative polarisation. The total reduction in the in-pore anion population across this range is by a factor of approximately 0.5. Integration of the total current shows that a very similar amount of charge is stored to the positive charging range (Fig. S2†). The reduction in the in-pore anion population could reflect the fact that the large cations are unable to access the pores, or have reduced mobility inside a significant proportion of the pores, and so expulsion of the smaller and more mobile anions provides a larger contribution to the charge storage process.

To further investigate the factors affecting the charge storage process, experiments were carried out on cells containing Li-TFSI and Na-TFSI electrolytes. In these systems, the anions are significantly larger than the cations, with the longest dimension of the TFSI anion being equal to 0.79 nm, whereas the Li^+ and Na^+ cations have diameters of 0.09 and 0.12 nm, respectively. However, the cations are expected to be strongly solvated with resulting estimated solvated diameters of 0.65 and 1.06 nm (assuming tetrahedral coordination of Li^+ to four ACN molecules, and octahedral coordination of Na^+ to six ACN molecules[54]).

The ^{19}F *in situ* NMR spectra and deconvoluted in-pore resonance intensities and shifts for electrodes containing 1.5 M Li-TFSI and Na-TFSI/ACN electrolytes are shown in Fig. 6. At 0 V, the resonances corresponding to the in-pore TFSI anions are observed at −85.1 and −84.4 ppm for the Li- and Na-based electrolytes, respectively. As the cells are charged, characteristic changes in the position and intensity of the in-pore resonance are observed, while the ex-pore/free electrolyte feature remains relatively unchanged. For both systems, an increase in the in-pore

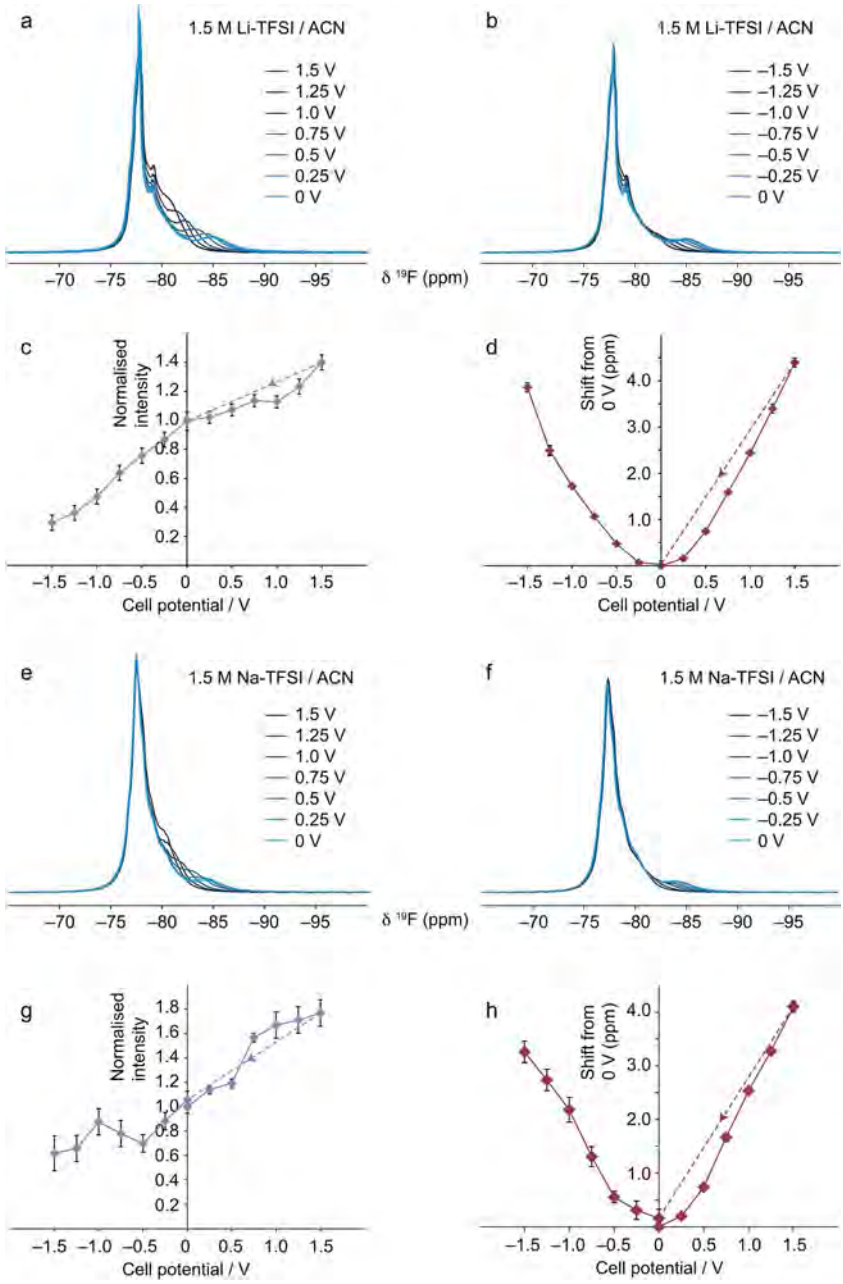


Fig. 6 ^{19}F *in situ* NMR spectra of supercapacitor electrodes containing (a) and (b) 1.5 M Li-TFSI/ACN and (e) and (f) 1.5 M Na-TFSI/ACN electrolytes charged to potentials between (a) and (e) 0 and 1.5 V and (b) and (f) 0 and −1.5 V. Deconvoluted in-pore resonance intensities and shift differences are shown for the LiTFSI electrolyte in (c) and (d), and for the Na-TFSI electrolyte in (g) and (h). Lines are added as guides for the eye. Dotted arrows indicate the 1.5 V → 0 V discharge step.

anion population is observed upon charging to 1.5 V. For Na-TFSI an abrupt increase is observed at 0.75 V, perhaps indicating a transition between two different charge storage processes as was observed for the 1.5 M NEt_4–BF_4/ACN electrolyte. At 1.5 V, the in-pore anion populations are increased by factors of 1.4 (Li-TFSI) and 1.8 (Na-TFSI) compared to at 0 V. The capacitances (Table 1) are very similar to the organic electrolytes, showing that a similar amount of charge is stored in both systems. Interestingly, the total shift change for the in-pore resonances over the positive voltage range is slightly larger for both of the TFSI-based electrolytes (4.1–4.4 ppm). This may indicate a chemical contribution to the change in NICS upon charging; it is possible that the anisotropic geometry of the TFSI anions could result in a different arrangement or proximity to the pore walls. Upon discharging to 0 V, the in-pore resonance intensity and shift returns to close to its original value for both systems. Over the negative voltage range, significant reductions in the in-pore resonance intensities are observed for both systems as anions are expelled from the pores. For the Li-TFSI electrolyte, a marked reduction is observed, and the in-pore anion population at −1.5 V is reduced to 0.3 times that at 0 V. For Na-TFSI, the reduction is less pronounced but still significant, with the anion population at −1.5 V being equal to 0.6 times the 0 V population, although the errors in this measurement are larger due to the low intensity of the in-pore resonance as compared to the ex-pore/free electrolyte feature. Negative polarization of the electrode in these systems clearly results in significant anion expulsion from the pores, in contrast to what was observed for the organic electrolytes. This indicates that there are additional factors that determine which ions undergo greater movement during charging, other than concentration and relative size effects.

Discussion

The results presented in this study offer a rare insight into one of the key questions regarding the mechanism of supercapacitance: what is the nature of the *ionic* charge that is developed within the micropores to balance the *electronic* charge developed on the electrode surface? The ^{19}F adsorption and 2D-EXSY measurements show that anions exist in equilibrium between the in-pore and ex-pore environments at zero applied potential. Assuming there is an equal number of in-pore anions and cations in order to maintain local charge neutrality at zero applied potential, this leads to a number of possible mechanisms for developing ionic charge within the micropores as the supercapacitor is charged, as shown schematically in Fig. 7. One possible mechanism is simply to expel co-ions, thereby leaving an excess of counter ions within the pores at a reduced overall packing density (Fig. 7a). Alternatively, it may be possible to adsorb counter-ions from outside the pores (Fig. 7b), thereby giving rise to a net ionic charge at an increased overall packing density, while the number of co-ions inside the pores remains unchanged. Finally, a third possible mechanism is ion exchange (Fig. 7c), whereby the combination of co-ion expulsion and counter-ion adsorption can give rise to a net ionic charge inside the pores, while the total ion population remains constant.

For all of the systems studied in this work, gravimetric capacitances of between 90–100 F g^{-1} were determined at 1.5 V, showing that the total amount of charge stored is very similar in each case. However, the *in situ* NMR results reveal that the

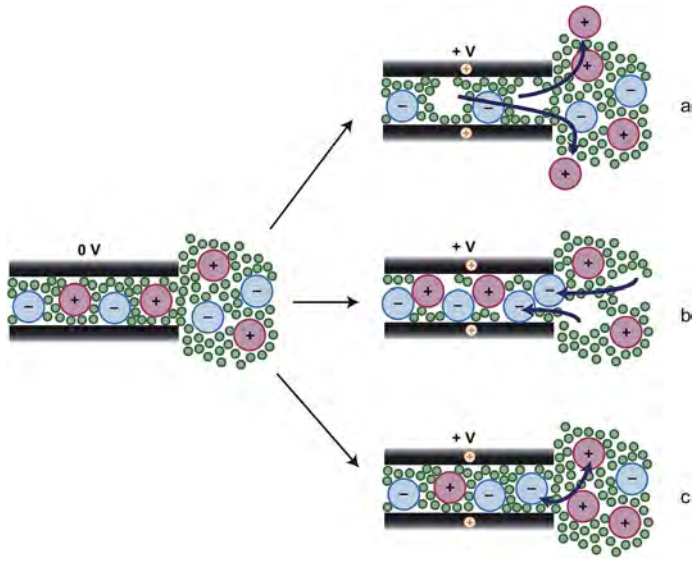


Fig. 7 Schematic illustrations of possible charge storage mechanisms for micropores that are wetted at zero potential. If the electrode surface is charged to a positive potential, an equal negative ionic charge can arise through either (a) the expulsion of cations from the pores, (b) adsorption of ex-pore anions into the pores, or (c) exchange of ex-pore anions for in-pore cations.

way in which the ionic charge is developed inside the micropores in the electrode as it charges differs depending on the properties of the electrolyte. The results obtained for the NEt_4–BF_4 electrolyte show that the ion concentration can significantly affect the way in which charge is stored when the electrode is positively polarized. The charge storage mechanism for the low concentration electrolyte seems to be dominated by anion adsorption, whereas for the high concentration electrolyte ion exchange takes place to a greater extent. In contrast, when the electrode is negatively polarized, the anion population was not found to change significantly for both concentrations, indicating that cation adsorption must be the main mechanism for charge storage. This cation adsorption-dominated mechanism in the negative charging regime will lead to an increased packing density within the pores. For the 1.5 M electrolyte, the NMR adsorption measurements show that solvated ions are already densely packed inside the pores at zero potential, taking up a volume that is comparable to the total pore volume. The adsorption of further ions into the pores upon charging will take up further space inside the pores. It therefore appears that desolvation must take place to some extent in order to accommodate the extra ions inside the pores.

The results obtained for the NBu_4–BF_4 electrolyte show that relative ion size also plays a role in determining the charge storage mechanism. In this case, the significantly larger NBu_4 cations seem to have difficulty accessing the smaller pores, forcing the expulsion of anions in the negative voltage range in order to balance the charge developed on the electrode surface. In the positive voltage range, the fact that large NBu_4 cations do not access the smaller, more confined environments within the electrode may also mean that they are more easily

expelled from the larger spaces that they occupy, with the result that the in-pore anion population has to increase by a smaller fraction.

The ^{19}F *in situ* NMR experiments on the Li- and Na-TFSI electrolytes indicate that other factors may also govern the charge storage process. In these systems, significant movement of the TFSI anions was observed in the positive and negative charging regimes. This is not consistent with the ion-size effect observed for the NEt_4–BF_4 and NBu_4–BF_4 systems, since the solvated anion and cation sizes are small enough in each case that they should both be able to access a large proportion of the pores. It is possible that other factors such as anion–cation association may also alter the charge storage mechanism. In the TFSI electrolytes, the high charge density of the cations may have caused them to 'carry' strongly associated anions out of the pores as they are expelled during negative polarization of the electrode. How significant this effect is, and whether there are other factors that determine which ionic species are adsorbed or expelled from the pores, requires further investigation through the study of a wider range of electrolyte systems. However, the results presented in this work show that the nature of the charge storage process in supercapacitor electrodes is not straightforward and does not arise solely due to the adsorption of counter-ions at the electrode surface as is often assumed.

Conclusions

^{19}F NMR spectroscopy has been used to quantify anions in model supercapacitor electrodes, and to selectively observe changes in anion populations and local environments during charging. The results presented in this work provide a rare insight into the behaviour of electrolyte ions under such conditions. In particular, we are able to draw the following conclusions:

(1) For the electrolytes studied in this work, the observation of resonances corresponding to in-pore and ex-pore anions shows that they exist in equilibrium between these two environments in the electrode at zero applied potential. This is confirmed by ^{19}F 2D-EXSY experiments, which show that the exchange takes place between the in- and ex-pore environments on the timescale of tens of Hz.

(2) For the commonly-used NEt_4–BF_4 electrolyte, the charge storage mechanism for the negative polarization of a YP-50F electrode involves cation adsorption and no significant change in the in-pore anion population. The charge storage mechanism for positive polarization of the electrode involves a combination of anion adsorption and ion exchange, with anion adsorption favoured at low concentrations.

(3) The charge storage mechanism is altered by increasing the size of the cation, which forces the expulsion of anions upon negative polarization of the electrode.

In addition to concentration and ion size effects on the charging mechanism observed for the tetra-alkylammonium tetrafluoroborate electrolytes, experiments on the Li-TFSI and Na-TFSI electrolytes indicate that there are other factors governing the charging mechanism, which are not yet fully understood. Comparison of the behaviour of a wider range of electrolytes will enable a better understanding of the different factors governing the extent to which ions are adsorbed and expelled from the electrode under charging. Furthermore, the development of *in situ* NMR methods that can observe both anions and cations, and quantify them

in absolute terms, will enable a much more detailed picture of the charging mechanism to be obtained in each system. Indeed, this work is ongoing in our laboratory and will be reported elsewhere.

Acknowledgements

A.C.F., J.M.G., H.W., and C.P.G. acknowledge the Sims Scholarship (A.C.F.), EPSRC (*via* the Supergen consortium, J.M.G. and H.W.), and the EU ERC (*via* an Advanced Fellowship to C.P.G.) for funding. N.M.T. was supported by the Northeastern Center for Chemical Energy Storage and by Energy Frontier Research Center funded by the U.S. DOE, BES under Award no. DE-SC0001294. P.S. acknowledges the support from the European Research Council (ERC, Advanced Grant, ERC-2011-AdG, Project 291543-IONACES). A.C.F. and J.M.G. thank the NanoDTC Cambridge for travel funding. We thank Dr. Paul Bayley for the synthesis of the TFSI electrolyte salts.

References

1 B. E. Conway, *Electrochemical Supercapacitors: Scientific Fundamentals and Technological Applications*, Springer, New York, 1st edn, 1999.
2 J. R. Miller and A. F. Burke, *Electrochem. Soc. Interface*, 2008, **17**, 53.
3 P. Simon and Y. Gogotsi, *Nat. Mater.*, 2008, **7**, 845.
4 M. T. Alam, J. Masud, M. M. Islam, T. Okajima and T. Ohsaka, *J. Phys. Chem. C*, 2011, **115**, 19797.
5 W. J. Cho, C. G. Yeom, B. C. Kim, K. M. Kim, J. M. Ko and K. H. Yu, *Electrochim. Acta*, 2013, **89**, 807.
6 S. Li, K. L. Van Aken, J. K. McDonough, G. Feng, Y. Gogotsi and P. T. Cummings, *J. Phys. Chem. C*, 2014, **118**, 3901.
7 Y. Zhai, Y. Dou, D. Zhao, P. F. Fulvio, R. T. Mayes and S. Dai, *Adv. Mater.*, 2011, **23**, 4828.
8 J. Chmiola, G. Yushin, Y. Gogotsi, C. Portet, P. Simon and P.-L. Taberna, *Science*, 2006, **313**, 1760.
9 J. Chmiola, C. Largeot, P.-L. Taberna, P. Simon and Y. Gogotsi, *Angew. Chem., Int. Ed.*, 2008, **47**, 3392.
10 J. Huang, B. G. Sumpter and V. Meunier, *Chem. - Eur. J.*, 2008, **14**, 6614.
11 S. Kondrat and A. A. Kornyshev, *J. Phys. Chem. C*, 2013, **117**, 12399.
12 S. Kondrat, P. Wu, R. Qiao and A. A. Kornyshev, *Nat. Mater.*, 2014, **13**, 387.
13 C. Merlet, B. Rotenburg, P. A. Madden and M. Salanne, *Phys. Chem. Chem. Phys.*, 2013, **15**, 15781.
14 R. Burt, G. Birkett and X. S. Shao, *Phys. Chem. Chem. Phys.*, 2014, **16**, 6519.
15 M. V. Fedorov and A. A. Kornyshev, *Chem. Rev.*, 2014, **114**, 2978.
16 G. Feng and P. T. Cummings, *J. Phys. Chem. Lett.*, 2011, **2**, 2859.
17 D. Jiang, Z. Jin and J. Wu, *Nano Lett.*, 2011, **11**, 5373.
18 G. Feng, R. Qiao, J. Huang, S. Dai, B. G. Sumpter and V. Meunier, *Phys. Chem. Chem. Phys.*, 2011, **13**, 1152.
19 D. Henderson, *J. Colloid Interface Sci.*, 2012, **374**, 345.
20 C. Merlet, B. Rotenberg, P. A. Madden, P.-L. Taberna, P. Simon, Y. Gogotsi and M. Salanne, *Nat. Mater.*, 2012, **11**, 306.

21 K. Sharma, H. Z. Bilheux, L. M. H. Walker, S. Voisin, R. T. Mayes, J. O. Kiggans, S. Yiacoumi, D. W. DePaoli, S. Dai and C. Tsouris, *Phys. Chem. Chem. Phys.*, 2013, **15**, 11740.
22 S. Boukhalfa, L. He, Y. B. Melnichenko and G. Yushin, *Angew. Chem., Int. Ed.*, 2013, **52**, 1.
23 F. W. Richey, B. Dyatkin, Y. Gogotsi and Y. A. Elbad, *J. Am. Chem. Soc.*, 2013, **135**, 12818.
24 P. Ruch, R. Kötz and A. Wokaun, *Electrochim. Acta*, 2009, **54**, 4451.
25 M. D. Levi, G. Salitra, N. Levy, D. Aurbach and J. Maier, *Nat. Mater.*, 2009, **8**, 872.
26 S. Sigalov, M. D. Levi, G. Salitra, D. Aurbach and J. Maier, *Electrochem. Commun.*, 2010, **12**, 1718.
27 M. D. Levi, S. Sigalov, D. Aurbach and L. Daikhin, *J. Phys. Chem. C*, 2013, **117**, 14876.
28 W.-Y. Tsai, P.-L. Taberna and P. Simon, *J. Am. Chem. Soc.*, 2014, **136**, 8722.
29 R. K. Harris, T. V. Thompson, P. R. Norman, C. Pottage and A. N. Tretheway, *J. Chem. Soc., Faraday Trans.*, 1995, **91**, 1795.
30 R. K. Harris, T. V. Thompson, P. R. Norman and C. Pottage, *J. Chem. Soc., Faraday Trans.*, 1996, **92**, 2615.
31 R. K. Harris, T. V. Thompson, P. R. Norman and C. Pottage, *Carbon*, 1999, **37**, 1425.
32 K. Shen and T. Pietrass, *J. Phys. Chem. B*, 2004, **108**, 9937.
33 W. Sekhaneh, M. Kotecha, U. Dettlaff-Weglikowska and W. S. Veeman, *Chem. Phys. Lett.*, 2006, **428**, 143.
34 Q. Chen, J. L. Herberg, G. Mogilevsky, H.-J. Wang, M. Stadermann, J. K. Holt and Y. Wu, *Nano Lett.*, 2008, **8**, 1902.
35 R. J. Anderson, T. P. McNicholas, A. Kleinhammes, A. Wang, J. Liu and Y. Wu, *J. Am. Chem. Soc.*, 2010, **132**, 8618.
36 S. Mitani, C. Murakami, Y. Korai, Y. Minato, S. Ishimoto, S. Suematsu and K. Tamamitsu, *Electrochim. Acta*, 2013, **94**, 30.
37 L. Borchardt, M. Oschatz, S. Paasch, S. Kaskel and E. Brunner, *Phys. Chem. Chem. Phys.*, 2013, **15**, 15177.
38 H. Wang, T. K.-J. Köster, N. M. Trease, J. Ségalini, P.-L. Taberna, P. Simon, Y. Gogotsi and C. P. Grey, *J. Am. Chem. Soc.*, 2011, **133**, 19270.
39 A. C. Forse, J. M. Griffin, H. Wang, N. M. Trease, V. Presser, Y. Gogotsi, P. Simon and C. P. Grey, *Phys. Chem. Chem. Phys.*, 2013, **15**, 7722.
40 D. Sebastiani, *ChemPhysChem*, 2006, **7**, 164.
41 M. Kibalchenko, M. C. Payne and J. R. Yates, *ACS Nano*, 2011, **5**, 537.
42 P. Ren, A. Zheng, X. Pan, X. Han and X. Bao, *J. Phys. Chem. C*, 2013, **117**, 23418.
43 A. C. Forse, J. M Griffin, V. Presser, Y. Gogotsi and C. P. Grey, *J. Phys. Chem. C*, 2014, **118**, 7508.
44 M. Deschamps, E. Gilbert, P. Azais, E. Raymundo-Piñero, M. R. Ammar, P. Simon, D. Massiot and F. Béguin, *Nat. Mater.*, 2013, **12**, 351.
45 H. Wang, A. C. Forse, J. M. Griffin, N. M. Trease, L. Trognko, P.-L. Taberna, P. Simon and C. P. Grey, *J. Am. Chem. Soc.*, 2013, **135**, 18968.
46 G. Laudisio, R. K. Dash, J. P. Singer, G. Yushin, Y. Gogotsi and J. E. Fischer, *Langmuir*, 2006, **22**, 8945.
47 D. G. Cory and W. M. Ritchey, *J. Magn. Reson.*, 1988, **80**, 128.

48 D. Massiot, F. Fayon, M. Capron, I. King, S. Le Calvé, B. Alonso, J.-O. Durand, B. Bujoli, Z. Gan and G. Hoatson, *Magn. Reson. Chem.*, 2002, **40**, 70.
49 Information available at http://www.kuraraychemical.com/products/sc/SCcarbon.htm.
50 Y. Gogotsi, P. Simon, C. Largeot, C. Portet, J. Chmiola and P.-L. Taberna, *US Pat.*, US0182000A1, 2011.
51 M. Fukano, T. Fujimori, J. Ségalini, E. Iwama, P.-L. Taberna, T. Iiyama, T. Ohba, H. Kanoh, Y. Gogotsi, P. Simon and K. Kaneko, *J. Phys. Chem. C*, 2013, **117**, 5752.
52 M. H. Levitt, *Spin Dynamics*, Wiley, Chichester, 1st edn, 2001.
53 M. E. Light, P. A. Gale and M. B. Hursthouse, *Acta Crystallogr.*, 2001, **E57**, o705.
54 D. Spångberg and K. Hermansson, *Chem. Phys.*, 2004, **300**, 165.

Ion Counting in Supercapacitor Electrodes using NMR Spectroscopy

John M. Griffin,*[1] Alexander C. Forse,[1] Hao Wang,[1] Nicole M. Trease,[2]

Pierre-Louis Taberna,[3] Patrice Simon,[3] and Clare P. Grey[1,2]

Supporting Information

S1. Spectral deconvolutions: ^{19}F NMR adsorption study

Deconvolutions for the ^{19}F NMR spectra of 4 mg pieces of YP-50F film soaked in different amounts of NEt_4-BF_4 electrolyte (Figures 1a and 1c in the main text) are shown in Figure S1. Deconvolution parameters for each fitted lineshape are summarized in Table S1.

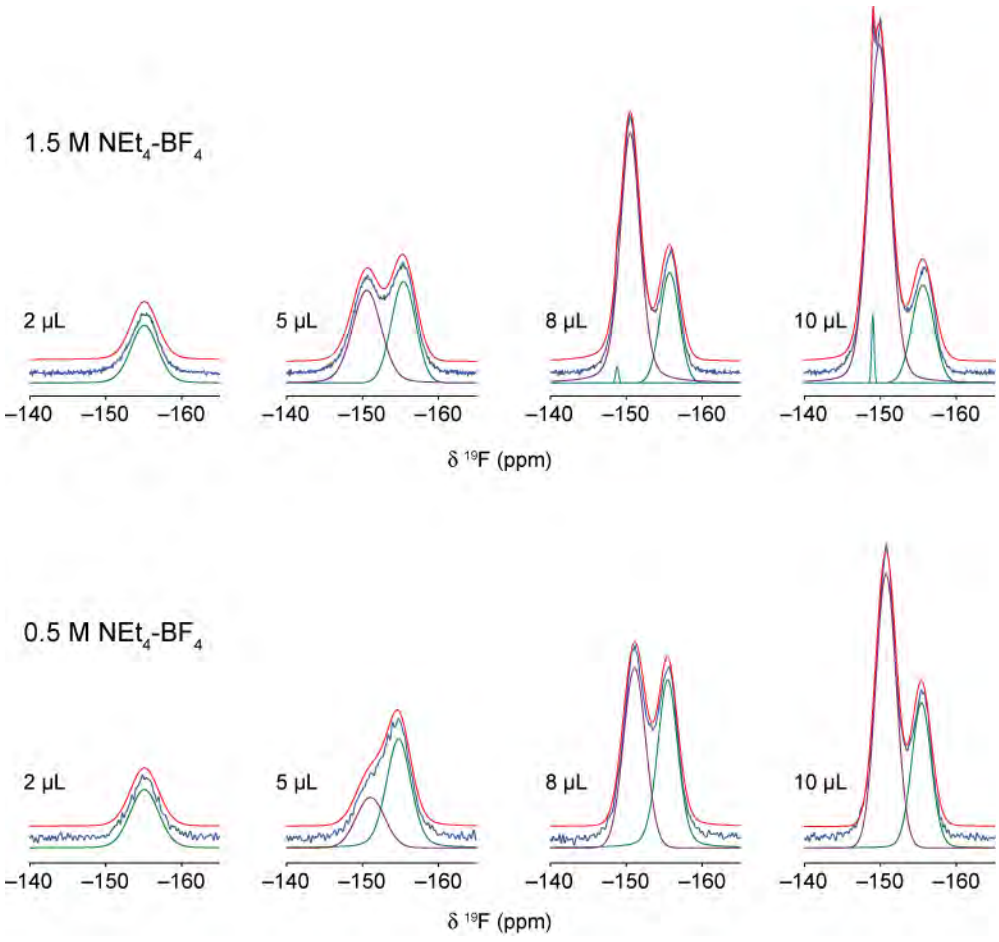


Figure S1. Deconvolutions of ^{19}F NMR spectra recorded for 4 mg pieces of YP-50F film soaked in different amounts of NEt_4-BF_4 electrolyte. Experimental lineshapes are shown in blue, individual fitted components are shown in green and purple, and the total fitted lineshape is shown in red.

Table S1. Deconvolution parameters for fits shown in Figure S1.

Volume /µL	Resonance	Shift (ppm)	Width (ppm)	G/L ratio	Absolute integrated intensity (arb.)	Relative integrated intensity*
1.5 M concentration						
2	in-pore	-155.09	4.19	0.83	62598	0.16
5	in-pore	-155.40	3.75	1.00	92204	0.24
	ex-pore	-150.57	4.45	0.84	106621	0.28
8	in-pore	-155.71	2.99	1.00	79599	0.21
	ex-pore 1	-150.51	3.11	0.69	212061	0.55
	ex-pore 2	-148.79	0.46	1.00	1874	0.00
10	in-pore	-155.59	3.40	1.00	80544	0.21
	ex-pore 1	-149.83	3.42	0.83	298478	0.77
	ex-pore 2	-148.99	0.40	1.00	6618	0.02
0.5 M concentration						
2	in-pore	-155.10	4.45	0.25	24952	0.21
5	in-pore	-154.76	3.81	0.77	41882	0.35
	ex-pore	-151.04	4.41	1.00	20341	0.17
8	in-pore	-155.45	3.12	0.77	51856	0.43
	ex-pore	-151.08	3.44	1.00	56501	0.47
10	in-pore	-155.40	3.02	0.92	41294	0.34
	ex-pore	-150.72	3.17	1.00	79424	0.66

*Integrated intensity relative to the total intensity of the 10 µL spectrum for each concentration.

S2. Spectral deconvolutions: In Situ NMR studies of supercapacitor cells

Representative deconvolutions of ^{19}F *in situ* NMR spectral recorded for cells held at 0 V are shown in Figure S2. In each case, a single component was used to model the in-pore resonance, while a minimum of 3 - 4 components were required to accurately model the ex-pore / free electrolyte feature. For Li-TFSI, more components were required owing to the more complex appearance of the ex-pore / free electrolyte feature.

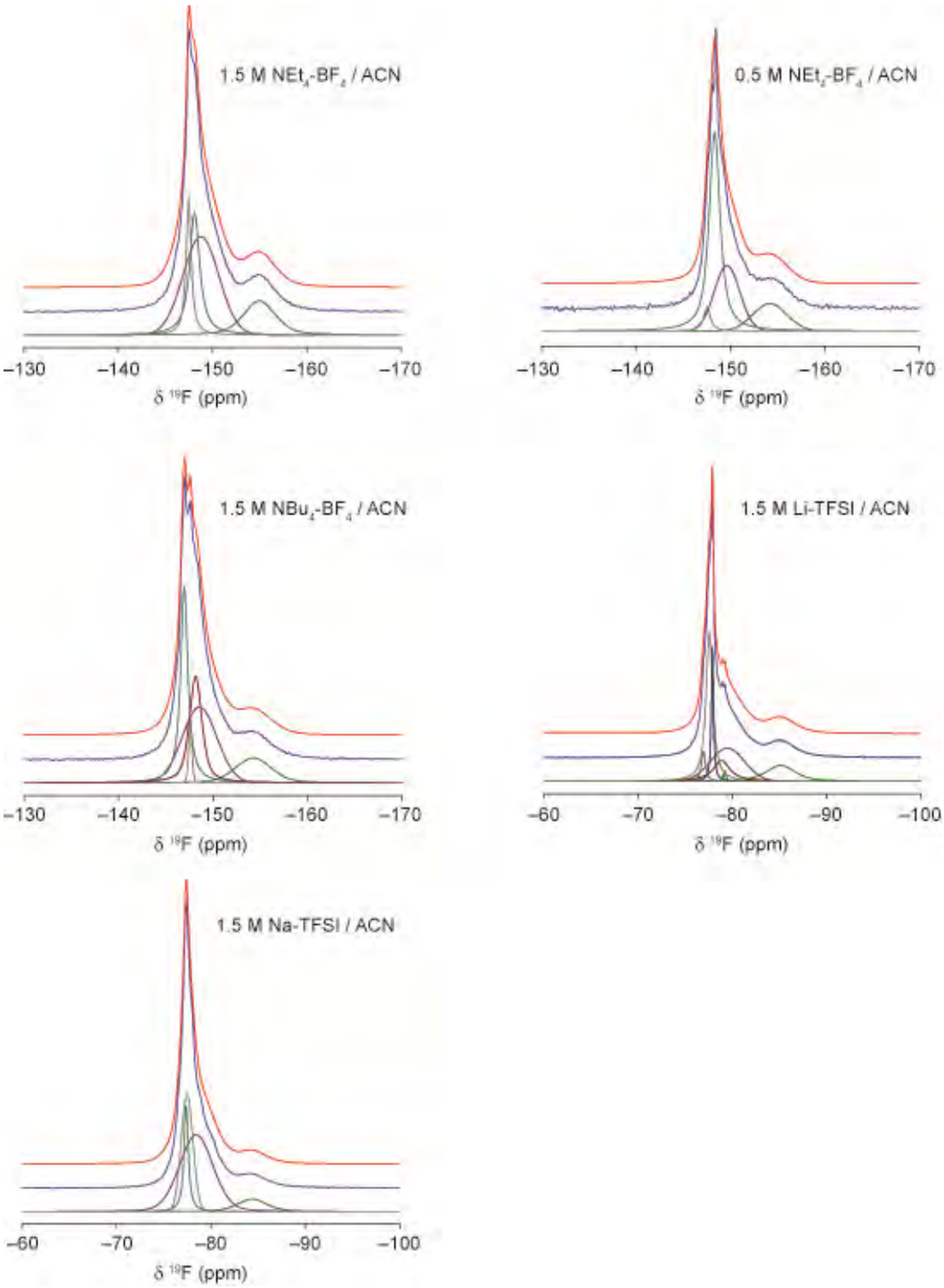


Figure S2. Representative deconvolutions of ^{19}F in situ NMR spectra recorded for cells held at 0 V. Experimental lineshapes are shown in blue, while the sum of individual fitted components is shown in red.

S3. Charge stored during *in situ* NMR experiments

Figure S3 shows the cumulative charge stored for each cell at each voltage step in the ^{19}F *in situ* NMR experiments. The stored charge varies approximately linearly with the applied cell voltage in each case and is fully discharged during the 1.5 V → 0 V step.

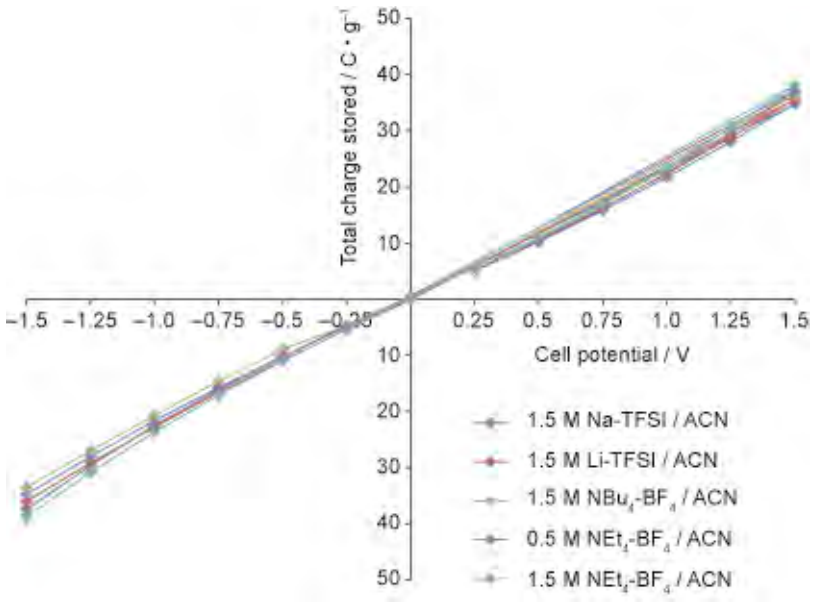


Figure S3. Plot showing cumulative charge stored as a function of voltage in supercapacitor bag cells used in *in situ* NMR experiments.